American Journal of Pathology, Vol. 165, No. 4, October 2004

Molecular Pathogenesis of Genetic and Inherited Diseases

A Novel *in Vivo* Lecithin-Cholesterol Acyltransferase (LCAT)-Deficient Mouse Expressing Predominantly LpX Is Associated with Spontaneous Glomerulopathy

Xianghong Zhu,* Andrew M. Herzenberg,† Mohammad Eskandarian,* Graham F. Maguire,* James W. Scholey,‡ Philip W. Connelly,* and Dominic S. Ng*

From the Department of Medicine, St. Michael's Hospital, Toronto, Ontario; the Department of Pathology,† University Health Network and University of Toronto, Toronto, Ontario; and the Department of Medicine,‡ University of Toronto, Toronto, Ontario, Canada*

Complete lecithin cholesterol acyltransferase (LCAT) deficiency is a rare genetic cause of extreme reduction in high density lipoproteins and there is a high prevalence of chronic renal dysfunction that may progress to renal failure. Previous *in vitro* studies suggest the vesicular lipoprotein X (LpX) particles commonly seen in LCAT-deficient plasmas may be causative. To test this hypothesis, we have generated a novel murine model that selectively accumulate LpX in the circulation by cross breeding the sterol regulatory element binding protein (SREBP) 1a transgenic mice (S+) with the LCAT knockout (lcat−/−) mice. Fast protein liquid chromatography fractionation of pooled plasma lipids revealed that virtually all cholesterol is concentrated in the very low density lipoprotein (VLDL)-sized fractions. These fractions are enriched in free cholesterol and phospholipid but extremely poor in triglyceride. Electron microscopy of the d <1.063 g/ml fraction of the S+lcat−/− mice revealed abnormal large vesicular particles, suggestive of LpX. The S+lcat−/− mice developed glomerular lesions spontaneously evident at 6 months with glomerular and tubulointerstitial lipid-deposits. Immunohistochemical staining with RhoA showed marked positive focal staining in glomeruli in the S+lcat−/− mice and undetectable in the S+/lcat+/+ control. By 10 months of age, the kidneys showed progressive glomerular injury including segmental foam cell infiltrates, mesangial expansion, and hyalinosis. Renal abnormalities are very similar to those seen in human LCAT deficiency. We conclude that the selective high-level accumulation of plasma LpX in the S+lcat−/− mice is strongly associated with a spontaneous glomerulopathy, providing *in vivo* evidence that LpX contributes to the LCAT deficiency-related nephropathy. *(Am J Pathol 2004, 165:1269–1278)*

Lecithin cholesterol acyltransferase (LCAT) deficiency is a rare monogenic disorder causative of severe plasma high density lipoprotein (HDL) deficiency. It has been well established that LCAT mediates the transfer of the *sn-2* fatty acyl moiety in phosphatidylcholine (PC) to the hydroxyl group of cholesterol. This reaction occurs predominantly on the HDL particles but significant LCAT activity has also been documented in non-HDL lipoprotein particles.[1,2] This reaction is central to the reverse cholesterol transport pathway in HDL metabolism[3] and a deficiency of the enzyme activity results in a reduction in plasma HDL-cholesterol (HDL-C) levels in a concentration-dependent manner. The residual plasma HDL is characterized by an accumulation of disk-shaped preβ HDL that may form the characteristic rouleaux on electron microscopy.[4,5] Other lipid phenotypes include an increase in plasma free cholesterol to esterified cholesterol (FC/CE) ratio, modest fasting hypertriglyceridemia, morphologically abnormal low density lipoprotein (LDL) and very low density lipoprotein (VLDL) particles and the formation of FC- and phospholipid (PL)-rich but triglyceride-poor vesicles known as lipoprotein X (LpX).[4,6] These vesicles, with the buoyant density in the LDL range but

Supported by grant NA4124 from the Heart and Stroke Foundation of Ontario, Canada (D.S.N.) and grant 45723 from the Canadian Institute for Health Research New Emerging Team (A.M.H. and J.W.S).

X.Z. and A.M.H. each contributed equally to this work.

Accepted for publication June 21, 2004.

Address reprint requests to Dominic S. Ng, St. Michael's Hospital West Annex 2–015, 38 Shuter Street, Toronto, Ontario M5B 1A6 Canada. E-mail: ngd @smh.toronto.on.ca.

the physical sizes in the range or larger than VLDL, also contain a small amount of albumin, CE, apolipoproteins (apo) C and E but are devoid of the structural protein apoB.[7] The clinical phenotype of complete LCAT deficiency is characterized by clouding of the cornea, mild anemia, and chronic progressive glomerulopathy.[8,9]

Glomerulopathy is highly prevalent in subjects with complete LCAT deficiency.[8] The natural history is characterized by a chronic progressive proteinuria. In many instances, the proteinuria and renal insufficiency may remain asymptomatic for decades, but in some, accelerated progression to renal failure have been reported.[9] Renal biopsy in patients with familial LCAT deficiency has shown mesangial expansion, lipid accumulation, and foam cell infiltrates in the capillary walls and in the mesangium.[10] Electron microscopy has shown membrane-like lamellar osmiophilic deposits in the glomerular basement membrane, subepithelially, subendothelially, and in the mesangium.[10,11] The underlying etiology of the glomerulopathy remains unclear and animal models emulating the spontaneous nephropathy seen in familial human LCAT deficiency have not been available. Anecdotal evidence in clinical observations implicated an association between the presence of LpX and the development of glomerulopathy.[8]

In LCAT-deficient humans, the plasma LpX level, when present, can be significantly lowered by reducing dietary fat intake. However, the mechanism for the generation of LpX in LCAT deficiency remains poorly understood. *In vitro* experiments examining cultured mesangial cells incubated with LpX are supportive of the notion that LpX may be causative of the nephropathy seen in LCAT-deficient subjects. Lynn et al.[12] reported an upregulation of monocyte chemoattractant protein-1 (MCP-1) mRNA and increased nuclear activities of NFκB in a mesangial cell culture system, suggesting that LpX may induce a pro-inflammatory response in the mesangial cells. A recent *in vivo* study using the LCAT knockout mouse as model reported that high fat diet treatment resulted in not only hyperlipidemia, but also the presence of LpX. Despite being homogeneous in their genetic background, only a proportion of the treated animals have detectable LpX by a radio-diffusion assay and a concordance in the detection of histological lesions.[13] While suggestive, the role of LpX in the development of glomerular lesions in this model may be confounded by the co-existing diet-induced hyperlipidemia.[13] To obtain more specific *in vivo* evidence for the causative role of LpX, it is of great interest to create an LCAT-deficient mouse model that eliminates all other circulating lipoprotein fractions but, at the same time, accumulates significant LpX in blood. In light of a recent report by Elferink et al,[14] demonstrating that LpX may be hepatic in origin, we hypothesize that breeding the lcat knockout mice into the sterol regulatory element binding protein (SREBP)1a transgenic mouse background may fulfill this goal. The SREBP1a-transgenic (S+) mice were generated with a constitutive overexpression of the NH_2-terminus segment of the SREBP1a variant, resulting in a dramatic increase in hepatic lipogenesis and overproduction of VLDL. Surprisingly, these mice sustain a normal circulating level of lipoproteins caused by a marked compensatory up-regulation of the LDL receptors, mediating the uptake of the apoB-containing lipoproteins. We therefore hypothesize that in the S+ mice made LCAT deficient, the apoB-containing lipoproteins overproduced would be cleared by the liver through the LDL receptors but, because of the LCAT deficiency, the LpX particles would be generated from the excess PL and FC and accumulate in proportion to the extent of VLDL overproduction.

We report that cross breeding the S+ and lcat−/− mice generates a novel murine model of complete LCAT deficiency with the plasma lipids being essentially FC- and PL-rich LpX vesicles. These "LpX" mice develop progressive glomerulopathic lesions that show light microscopic and ultrastructural abnormalities similar to those seen in human LCAT deficiency-associated nephropathy.

Materials and Methods

Animals

Lcat−/− mice, in a C57Bl/6xsv129 background, were maintained in our laboratory through brother-sister mating as previously reported.[15] SREBP 1a transgenic mice (S+),[18] bred into the C57Bl/6JxSJL background[16] were purchased from Jackson Laboratories (Bar Harbor, ME). The S+ lcat−/− double-mutant mice were generated by first cross-breeding the S+ mice with lcat−/− to yield S+ (hemizygotes)lcat+/−. Brother-sister mating was carried out for four additional generations before any animal to be used for further breeding for this study. Littermate S+lcat+/+ mice were used as controls. The presence of the human truncated SREBP 1a transgene (S+ genotype)[17] was determined by tail DNA PCR (forward primer: AGGCAGCTTGTCTCCACCT and reverse primer: GGAGGGCTTCCTGTAGAGA) and the lcat genotypes were determined by tail DNA PCR as previously reported.[15] All studies were carried out with the mice being fed a chow diet and littermates were used as controls. All mouse protocols were approved by the Animal Care Committee at St. Michael's Hospital, Toronto.

Plasma Lipid Analyses

Plasma lipid analyses were performed on mice 7 to 10 weeks of age after an overnight fast. Plasma was obtained as previously described.[15] The 1.019–1.063 g/ml ("LDL") fraction was obtained by ultracentrifugation. Fast protein liquid chromatography (FPLC) fractionation on total plasma and the "LDL" fraction was performed on a Superose 6HR column (10 mm × 30 cm) (Amersham Pharmacia Biotech, QC).[15] Plasma and Superose fractions were analyzed on an RA-1000 (Bayer Diagnostics) using enzymatic assays for total cholesterol, TG, glycerol blank, FC, and PL.

Table 1. Fasting Lipid Profile of S+lcat−/− and S+lcat+/+ Control Mice

	T Chol	Trig	FC	PL	FC/CE
			mmol/L		
S+lcat−/−	1.93 ± 0.91	0.00 ± 0.06	1.01 ± 0.61	1.32 ± 0.47	1.18 ± 0.57
S+lcat+/+	1.50 ± 0.35	0.19 ± 0.10	0.22 ± 0.02	1.42 ± 0.08	0.18 ± 0.08

$n = 5$ for each genotype.

Renal Function

Serum creatinine levels were determined on S+lcat−/−, and control S+lcat+/+ and S-lcat−/− mice at 6 to 7 months of age. Serum obtained from individual animals by tail bleeding were analyzed for creatinine level using the Kodak Ektachem Clinical Chemistry kit (Ortho Clinical Diagnostics).

Electron Microscopy

Electron microscopy of the lipoproteins were performed on the plasma d <1.063 g/ml fractions pooled from three animals from each genotype. Samples were spread on a carbon grid and stained with 2% phosphotungstic acid at pH 6.8 and examined with a Hitachi 7000 transmission electron microscope.

Histochemistry and Histopathology

Mice were sacrificed at 6 to 7 months and 10 to 11 months of age. After perfusion with saline, kidneys were quickly dissected and cut into smaller fragments. Portions of the specimens were fixed in 10% buffered formalin and paraffin-embedded. Histological sections were cut at 3 μm and stained with hematoxylin-eosin and periodic acid Schiff reaction. Cryosections were obtained by embedding tissues in OCT and snap-frozen in liquid nitrogen before sectioning. Oil-red-O was used for detection of neutral lipids in frozen sections. Cryosections were treated with 3% Oil-red-O followed by counterstaining with hematoxylin.

Immunostaining for RhoA in kidney sections was carried out using anti-RhoA polyclonal rabbit antibody (RhoA 119, catalog no. sc-179, Santa Cruz Biotechnology, Santa Cruz, CA) at 1:2000 dilution. A biotinylated goat-anti-rabbit IgG secondary antibody (Vector) was used for immuno-detection with DAB (Vector). Immunostaining for macrophages in kidney sections were carried out using an anti-mouse MAC-3 monoclonal antibody (Cedarlane Lab Ltd, Ontario, Canada) at 1:150 dilution. A biotinylated rabbit anti-mouse secondary antibody (Vector) was used for immunodetection with DAB (Vector).

Electron Microscopy of Mouse Kidneys

Tissue was fixed in buffered 1% glutaraldehyde-4% formaldehyde, post-fixed in 1% osmium tetroxide, and embedded in epon-araldite. Ultra-thin sections were stained with uranyl acetate and lead citrate and examined with a Jeol 1200 EX-II transmission electron microscope. Glomerular basement membrane thickness was measured by the harmonic mean of 50 orthogonal intercepts of the lamina densa.

Results

Production of the S+lcat−/− Mice

The S+, S+lcat+/− and S+lcat−/− double-mutant mice all bred normally. With the exception of hepatomegaly, all S+ mice with different lcat genotypes grew normally and appeared well up to at least 20 months of age.

Plasma Lipid and Lipoprotein Analyses

Lipoprotein analyses of the S+lcat−/− and S+lcat+/+ mice are summarized in Table 1 and Figure 1. Total plasma cholesterol in the S+lcat+/+ mice was lower than those of the wild-type mice, largely attributable to a significant reduction in HDL-C (FPLC fractions 14 to 21) as seen in Figure 1a, consistent with previous reports.[17] Despite LCAT deficiency, it is of interest to observe a persistent high level of plasma cholesterol with a concomitant near absence of plasma triglycerides in the S+lcat−/− mice.

Lipoprotein analyses on the FPLC fractions showed a significant reduction in cholesterol in all lipoprotein fractions in the S+lcat+/+ mice as compared with the S-lcat+/+ (wild-type) mice as previously reported[5] (Figure 1a). The reduction in the non-HDL fractions had been attributed to the compensatory up-regulation of the LDL receptors in the liver but the modest reduction in HDL-C is not well understood. By cross breeding the S+ mice into the LCAT knockout background, the HDL-C in the resultant double-mutant is severely reduced to a level similar to that of the lcat−/− mice[5] (Figure 1a). The cholesterol levels in the LDL/IDL fractions were further reduced when compared to the S+lcat+/+ mice but there was a large accumulation of cholesterol in the void, large "VLDL"-sized fractions. As seen in Figure 1, b to d, the large, VLDL-sized particles were virtually completely devoid of triglycerides. Rather, they are highly enriched in FC and PL. The elevated plasma levels of total FC and PL in the S+lcat−/− mice were found to be concentrated virtually entirely in the large "VLDL" fractions.

Electron Microscopy of Plasma Lipoproteins

Non-HDL plasma fractions (d <1.063 g/ml) were compared for lipoprotein morphologies (Figure 2). In the S+lcat+/+ samples, all particles were spherical and

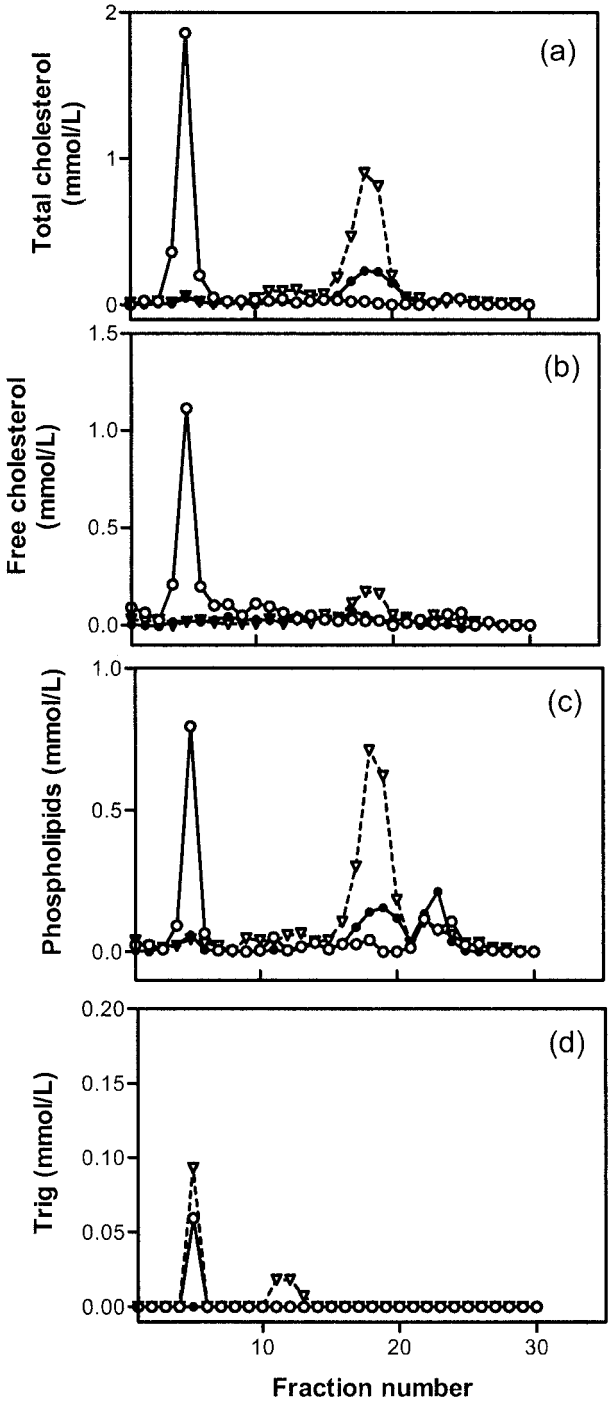

Figure 1. FPLC lipid profile of pooled plasmas ($n = 4$ each) from S+lcat−/− (**open circle**, **solid line**); S+lcat+/+ (**closed circle**, **solid line**), and S-lcat+/+ (**inverted triangle**, **broken line**).

were dominated by the LDL-sized particles. The samples from the S+lcat−/− mice, on the other hand, showed abundance of large-sized, irregularly shaped, vesicles that were entirely absent in the S+lcat+/+ mice. In light of the virtual absence of plasma triglycerides in the S+lcat−/− mice, these large vesicles are consistent with FC- and PL-rich LpX vesicles.

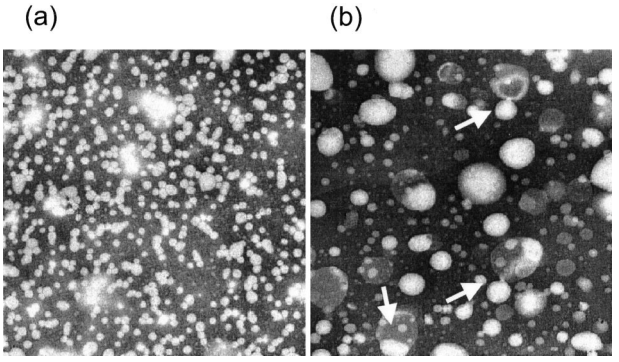

Figure 2. Electron micrograph of lipoprotein fractions at density <1.063 g/ml in pooled fasting plasma from S+lcat+/+ (**a**) and S+lcat−/− (**b**) groups.

Renal Function

Serum creatinine levels of the S+lcat−/− mice ($n = 4$) were not significantly different from the S+lcat+/+ mice ($n = 4$) at 6 to 7 months (mean ± SD: 27.8 ± 5.0 μmol/L versus 23.5 ± 5.9 μmol/L; $P = 0.32$) and from the age-matched S-lcat−/− mice ($n = 6$) (mean ± SD: 27.8 ± 5.0 μmol/L versus 22.3 ± 2.3 μmol/L; $P = 0.11$). To determine whether there were changes in kidney function accompanying the histological changes in the S+lcat−/− mice, urine was collected from 6-month-old S+lcat−/− ($n = 2$) and S+lcat+/+ mice ($n = 4$). Three μl of urine was subjected to SDS-PAGE and stained with Coomasie-Blue (Figure 3). Albumin was detected in urine samples from S+lcat−/− mice but S+lcat+/+ mice did not exhibit albuminuria (Figure 3).

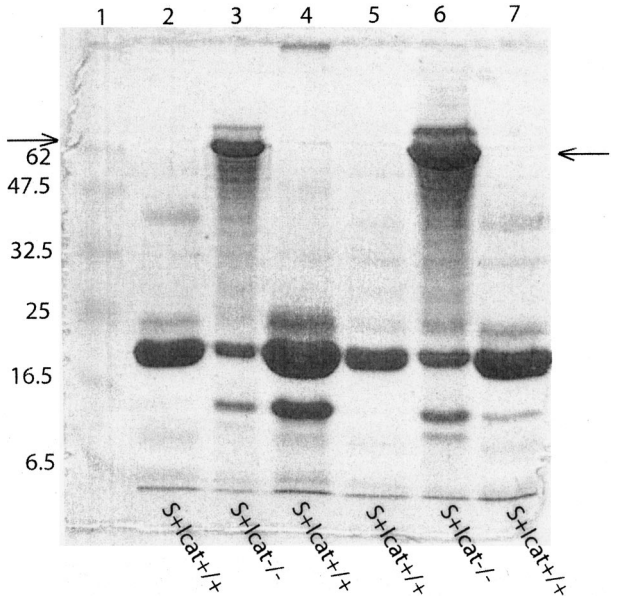

Figure 3. Sodium dodecyl sulfate polyacrylamide gel electrophoresis (SDS-PAGE) of mouse urine. Three μl of mouse urine from 6-month-old S+lcat−/− ($n = 2$) and age-matched S+lcat+/+ ($n = 4$) mice was subjected to SDS-PAGE and stained with Coomassie blue. Six-month-old S+lcat−/− mice showed an increased protein band (**lanes 3** and **6**, at level of the **arrows**) at approximately 68 kd, consistent with the development of albuminuria. **Lanes 2**, **4**, **5**, and **7** are urine from age-matched S+lcat+/+ littermate control mice, which show no albuminuria. **Lane 1** shows molecular weight markers in kd.

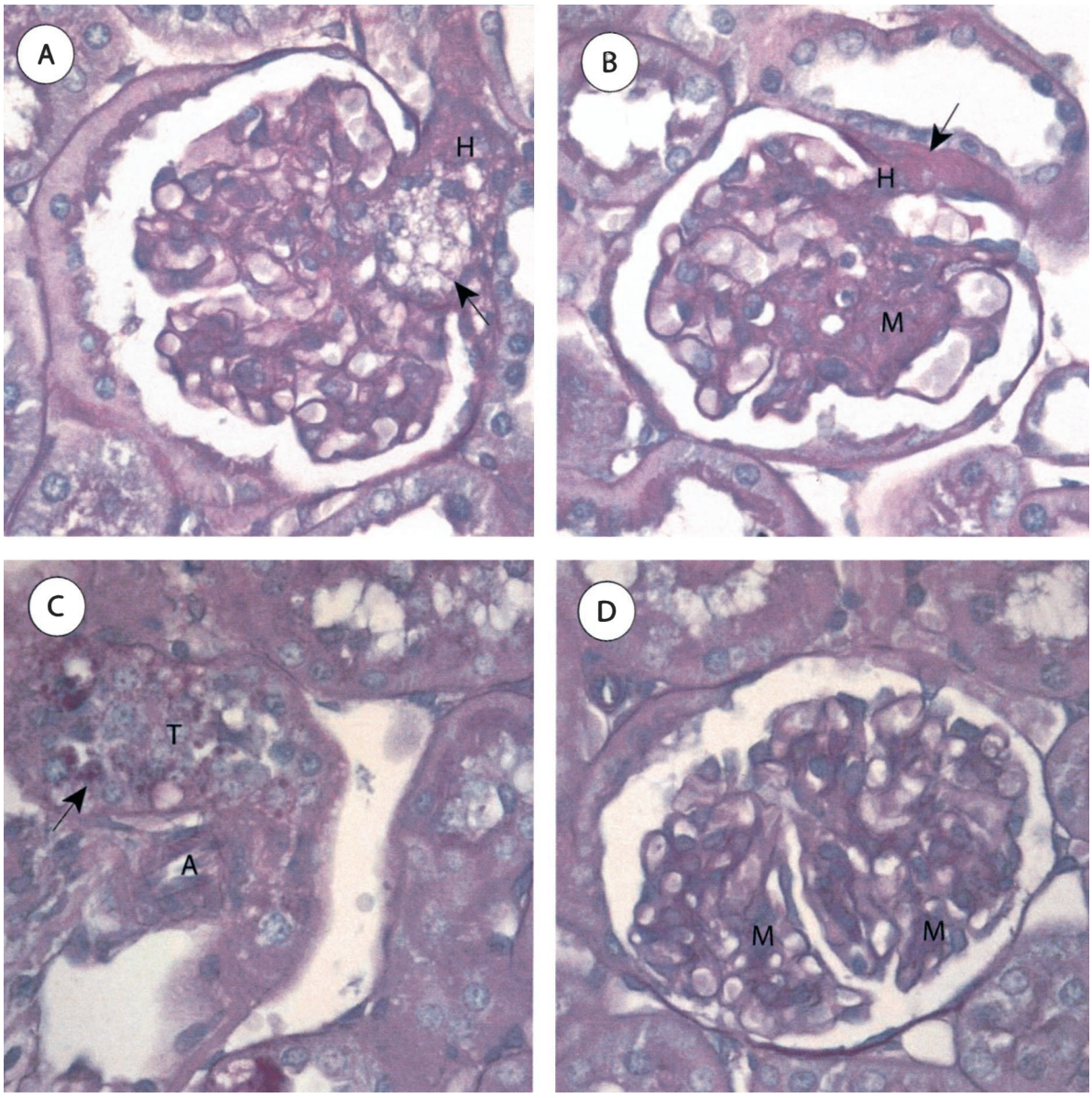

Figure 4. Light microscopic features of S+lcat−/− mouse kidneys. **A:** S+lcat−/− mouse showing segmental foam cell infiltrates (**arrow**) in the glomerular hilum and mild mesangial expansion (H, glomerular hilum). **B:** S+lcat−/− mice showing segmental marked mesangial matrix expansion and increased mesangial cellularity, and arteriolar hyalinosis (**arrow**) at the vascular pole (M, mesangium; H, glomerular hilum). **C:** S+lcat−/− mice showing proximal tubules. Proximal tubular epithelial cells contain intracellular proteinaceous re-absorption droplets (**arrow**). Extra-glomerular arterioles show no morphological abnormalities, particularly no hyalinosis (T, proximal convoluted tubule; A, arteriole). **D:** S+lcat+/+ mouse kidney showing focal mild mesangial expansion (M, mesangium). All periodic acid Schiff, original magnification, ×600.

Histopathology of the Kidneys: Light Microscopy

S+lcat−/− Mice

The S+lcat−/− mice (n = 4) showed no gross abnormalities and normal architecture of the tubulointerstitium in the cortex and medulla. The renal, arcuate, and interlobular arteries showed no atherosclerosis. The S+lcat−/− mice showed segmental foam cell infiltrates in approximately 25% of glomeruli. The foam cell infiltrates preferentially involved the glomerular vascular poles in approximately 60% of involved glomeruli (Figure 4A). These mice also showed a diffuse moderate increase in mesangial matrix and a diffuse mild to moderate and focally marked increase in mesangial cellularity, occasionally forming mesangial nodules (Figure 4B). Many glomerular capillary loops showed decreased patency due to mesangial encroachment. There was no endocapillary proliferation. The capillary walls appeared mildly thickened on periodic acid Schiff stain. There was diffuse glomerular arteriolar hyalinosis. Some of the proximal tubular epithelial cells exhibited intracellular protein re-absorption droplets (Figure 4C).

S+lcat+/+ Mice

To document that the renal phenotype seen in S+lcat−/− mice was not due solely to the effect of he-

patic SREBP1 overexpression, the primary comparison of the S+lcat−/− mice was made with 10-month-old S+lcat+/+ mice ($n = 6$). The gross and light microscopic low-power architecture of the kidneys was normal in these mice. No globally sclerosed glomeruli were identified. The interlobular and arcuate arteries were unremarkable and showed no atherosclerosis. There was no interstitial fibrosis or tubular atrophy. The glomeruli (Figure 4D) showed focal mild mesangial matrix expansion and occasional foci of mild mesangial hypercellularity. Apart from these focal changes, the glomeruli were otherwise unremarkable and comparable to 12-month-old wild-type (S-lcat+/+) C57-Bl/6 mouse kidneys. The capillary loops were patent and the capillary walls were of normal thickness. No foam cells were identified. There were occasional foci of mild arteriolar hyalinosis.

S-lcat−/− Mice

The low-power architecture, tubulointerstitium, and arteries were normal by light microscopy in 10-month-old S-lcat−/− mice ($n = 2$) and comparable to wild-type (S-lcat+/+) C57-Bl/6 mice. There was no atherosclerosis. The glomeruli showed occasional foci of mild mesangial expansion and foci of glomerular hilar arteriolar hyalinosis. No foam cell infiltrates were identified by light microscopy (data not shown).

Oil-Red-O Staining of S+lcat−/− Mouse Kidneys

At 10 months of age, Oil-red-O staining of the cryosections showed large focal accumulation of neutral lipids in >50% of the glomeruli in the S+lcat−/− mice (Figure 5A) but were completely absent in the age-matched S+lcat+/+ mice (Figure 5B). Similar neutral lipid deposits were also detected in the S+lcat−/− mice at 6 months albeit considerably less prevalent, and these findings were completely absent in the S+lcat+/+ mouse kidneys.

Immunohistochemistry

Rare, large-sized MAC-3-positive foam cells were detected in a S+lcat−/− mouse glomerulus at 6 months (Figure 5C) but none observed at 10 months of age. Immunohistochemical staining for murine MAC-3 was completely negative in the S+lcat+/+ mouse kidneys (Figure 5D).

Immunohistochemical staining of the kidney sections for RhoA was found to be positive and distributed focally near the vascular pole in the S+lcat−/− mouse glomeruli at 6 months (Figure 5E) but was completely absent in the age-matched S+lcat+/+ mice (Figure 5F). Staining for RhoA appears mostly in the wall of the glomerular hilar arterioles, primarily in the vascular smooth muscle cells. At 10 months, a larger proportion of glomeruli (33.7%) in the S+lcat−/− mice stained positive for RhoA but the distribution remained localized to the vascular pole. A much smaller proportion (7.4%) of the S+lcat+/+ mouse glomeruli also stained positive for RhoA.

Renal Ultrastructure

Electron microscopy of 6-month-old S+lcat−/− mice showed numerous mesangial membrane-like lamellar osmiophilic dense inclusions (Figure 6A). Most glomerular capillary loops showed endothelial osmiophilic inclusions at 6 months. The S+lcat−/− mice showed evidence of progression from 6 to 10 months of age in the form of fewer lipid deposits, evidence of chronic mesangial injury, and progressive glomerulosclerosis. At 10 months of age, S+lcat−/− mice showed qualitatively fewer mesangial electron dense inclusions than at 6 months (Figure 6B). Ten-month-old mice showed mesangial hyalinosis in several foci, suggestive of plasma protein insudates due to endothelial or mesangial injury. Several glomerular visceral epithelial cells (podocytes) contained osmiophilic inclusions (Figure 6C). This finding was associated with localized foot process effacement adjacent to the inclusions. Podocyte effacement was not present at sites that were not adjacent to the osmiophilic inclusions. The glomerular basement membranes appeared normal thickness with a harmonic mean thickness of 191 nm.[17,18] At 10 months, S+lcat−/− mice showed ultrastructural evidence of tubulointerstitial accumulation of lipid deposits (Figure 6D). There were osmiophilic inclusions in proximal convoluted tubular epithelial cells, adjacent to tubular basement membranes, and in the cortical interstitium. Occasional interstitial foam cells were present, and these contained several small osmiophilic deposits.

Electron microscopy of 10-month-old S+lcat+/+ mice showed no abnormalities (Figure 7A). The ultrastructural features were comparable to those seen in 12-month-old wild-type C57Bl/6 mice (not shown). There were no osmiophilic inclusions. There were no mesangial alterations and podocytes were intact and not effaced. The glomerular basement membranes appeared normal thickness with a harmonic mean thickness of 174 nm.[17,18] Six-month-old S-lcat−/− mice showed a few mesangial and glomerular endothelial osmiophilic inclusions, many of which had a swirled lamellar appearance (Figure 7B). There were no podocyte, glomerular basement membrane, tubulointerstitial, or macrophage osmiophilic inclusions identified.

Figure 5. Histochemical and immunohistochemical staining of S+lcat−/− mouse kidneys. **A** and **B:** Oil-red-O stain for neutral lipids on frozen sections. **A:** Large neutral lipid deposits are seen in glomeruli and proximal tubular epithelial cells in the S+lcat−/− mice only (original magnification, ×400). **B:** Staining is absent from the S+lcat+/+ control mice at either 6 or 10 months (original magnification, ×200). **C** and **D:** Immunohistochemistry for macrophages (Mac 3 monoclonal antibody, immunoperoxidase and hematoxylin counterstain, original magnification, ×600). **C:** Mac 3 staining showing glomerular foam cells (**arrow**) in a 6-month-old S+lcat−/− mouse. **D:** Mac 3 staining showing of S+lcat−/− mice shows no foam cells. **E** and **F:** Immunohistochemistry for RhoA (RhoA polyclonal antibody, immunoperoxidase and hematoxylin counterstain, original magnification, ×200). **E:** RhoA immunostaining seen in S+lcat−/− glomeruli, showing preferential localization to the vascular pole (**arrows**). **F:** Immunohistochemistry for RhoA of S+lcat+/+ mice showing no staining for RhoA in the glomeruli at 6 months.

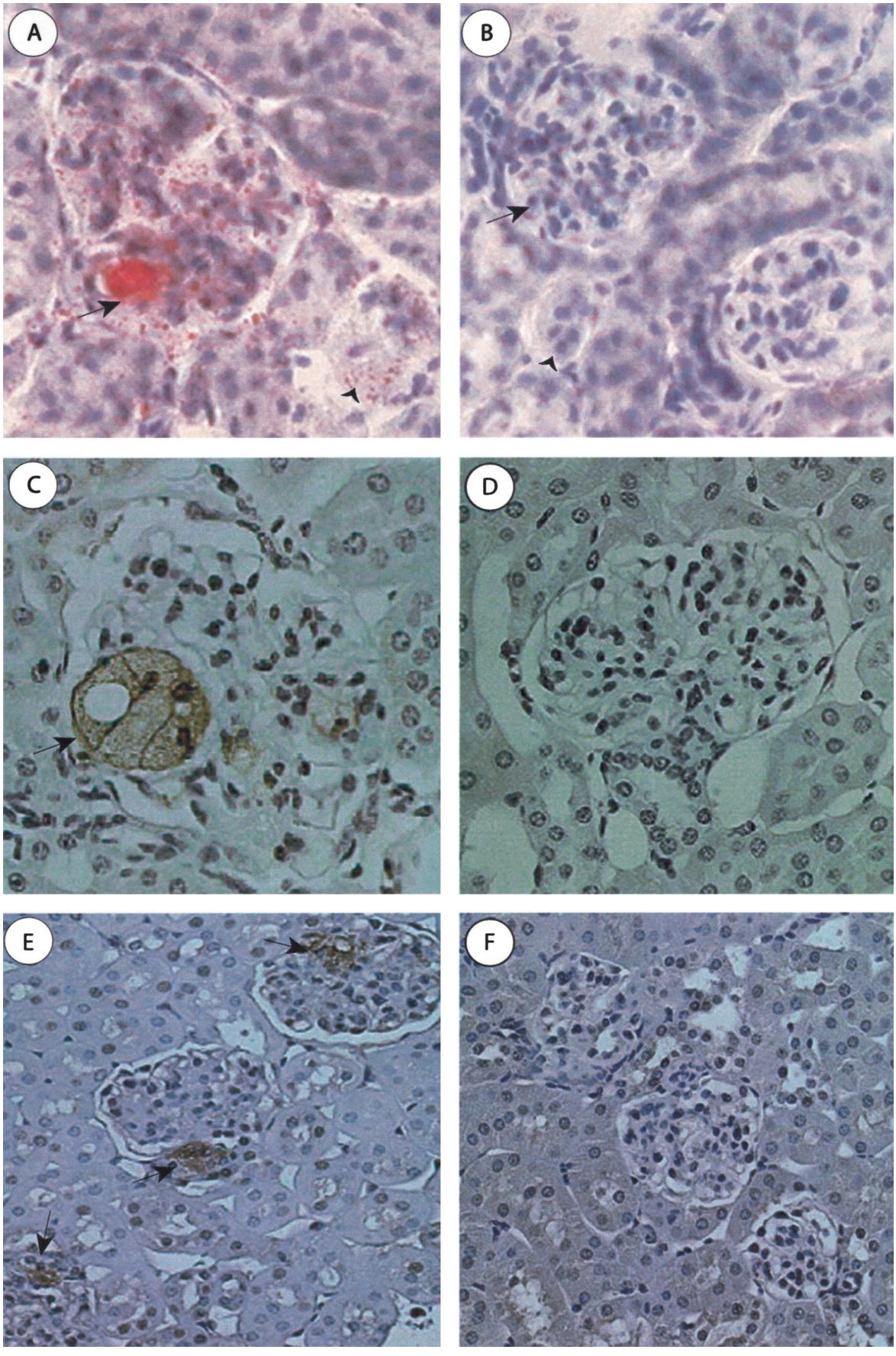
A
B
C
D
E
F

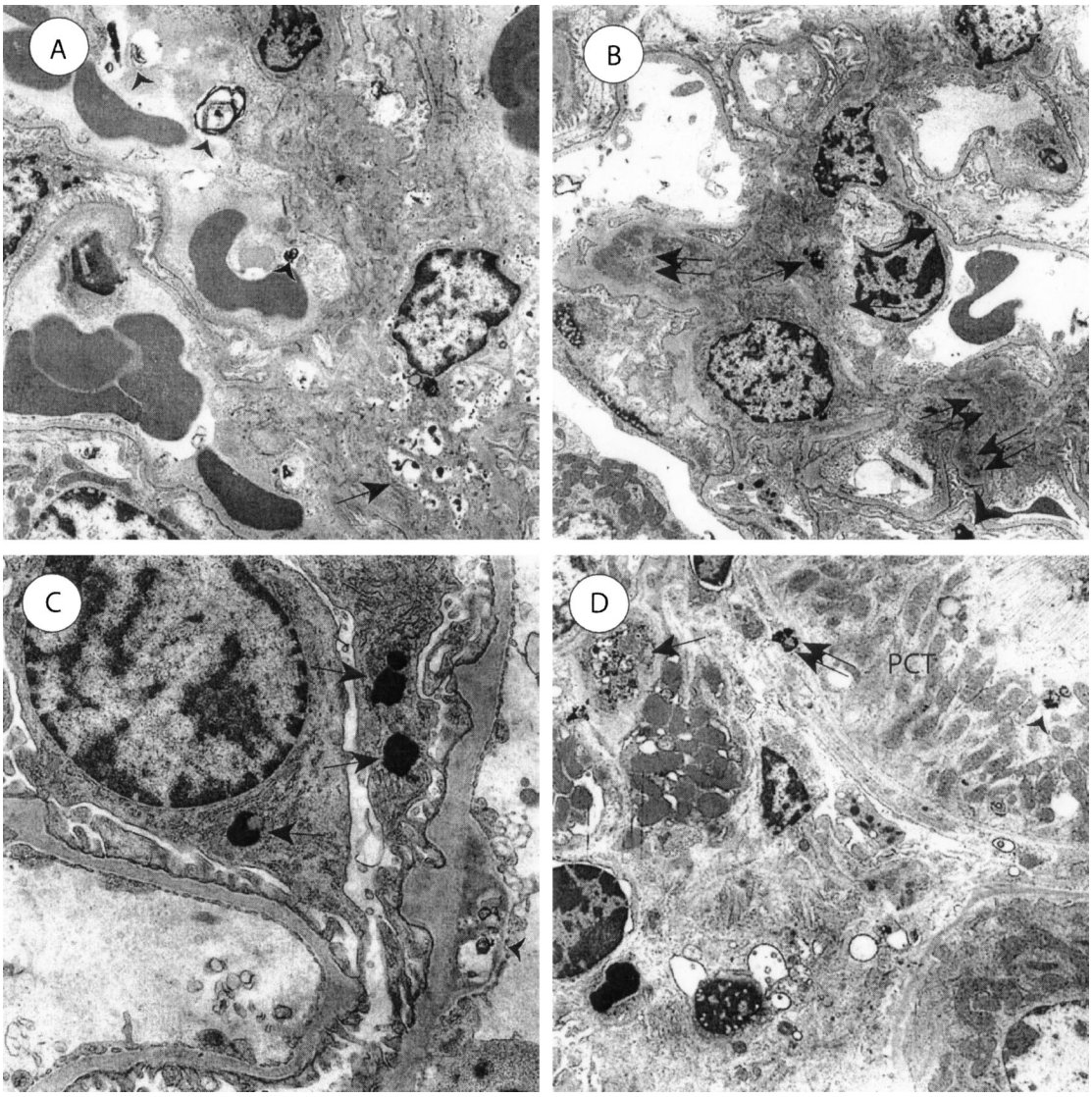

Figure 6. Electron microscopy of S+lcat−/− kidneys. **A:** Six-month-old S+lcat−/− kidneys show numerous mesangial (**arrow**) and glomerular endothelial (**arrowheads**) osmiophilic inclusions. There is mild mesangial matrix expansion. **B:** At 10 months of age, S+lcat−/− kidneys show fewer mesangial osmiophilic deposits (**single arrow**) compared to 6-month mice. However there is evidence of mesangial injury in the form of mesangial hyalinotic lesions (**double arrows**). Podocytes show osmiophilic inclusions (**arrowhead**) associated with focal foot-process effacement. **C:** Ten-month-old S+lcat−/− mice show foci with several osmiophilic inclusions in podocytes (**arrows**) with only minor localized foot process effacement. Osmiophilic inclusions are present in glomerular endothelial cells (**arrowhead**). **D:** Ten-month-old S+lcat−/− mice show tubulointerstitial electron-dense inclusions. Osmiophilic inclusions are present in proximal tubular epithelial cells (**arrowhead**), adjacent to tubular basement membranes (**double arrow**), and scattered through the interstitium. Occasional interstitial foam cells (**single arrow**) contain osmiophilic dense inclusions. (PCT, proximal convoluted tubular epithelial cell). Original magnification, ×3000 (**A**), ×2500 (**B**), ×8000 (**C**), and ×2500 (**D**).

Discussion

In this paper, we report for the first time the generation of a LCAT-deficient mouse model for which the circulating lipoproteins are predominantly LpX and that this mouse model develops spontaneous chronic glomerulopathy. Glomerulopathy is highly prevalent in human subjects with complete LCAT deficiency and is the main cause of morbidity and mortality in many affected subjects. However, the underlying pathogenesis remains elusive.

The light microscopic and ultrastructural features of the S+lcat−/− mouse kidneys are remarkably similar to those seen in familial human LCAT deficiency. This mouse model and the nephropathy seen in human LCAT-deficiency both show light microscopic mesangial matrix expansion, glomerular hilar foam cell infiltrates, and lipid deposits in the glomeruli and tubulointerstitium.[10] Ultrastructural features are also similar in both, showing lamellar osmiophilic deposits in the mesangium, in proximity to the glomerular basement membrane, and in the interstitium.[10,11] The S+lcat−/− mice show evidence of mesangial injury, mesangial matrix expansion, and glomerulosclerosis progressing from 6 to 10 months of age. This is also similar to that seen in human LCAT-deficiency nephropathy, where the lesions chronically are associated with progressive mesangial and glomerular sclerosis.[11]

Anecdotal evidence based on limited clinical studies of LCAT-deficient subjects suggested that LpX might be

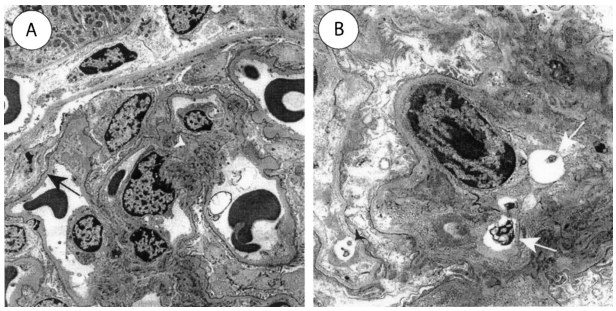

Figure 7. Electron microscopy of control mouse kidneys. **A:** Ten-month-old S+lcat+/+ mouse kidneys show no ultrastructural abnormalities. The glomerular basement membrane (**arrow**) is of normal thickness, there are no mesangial alterations, and there are no osmiophilic deposits. **B:** Six-month-old S-lcat−/− mouse kidneys show occasional osmiophilic inclusions in the mesangium (**arrows**) and in glomerular endothelial cells (**arrowhead**). Deposits are qualitatively much fewer in number than in S+lcat−/− mice. In addition, there are no electron-dense deposits in glomerular basement membrane or in podocytes. Original magnification, ×2000 (**A**), ×5000 (**B**).

causative for the renal disease. Recent *in vitro* experiments have also provided evidence of direct interaction of LpX with mesangial cells, resulting in proinflammatory changes.[12] More recently, histopathological changes were reported in a mouse model of LCAT deficiency.[13] LCAT knockout mice in a uniform C57Bl/6 background fed a high fat/high cholesterol diet were shown to develop hyperlipidemia. However, LpX was detected in only a proportion of these mice in the plasma, in association with histological changes in the kidneys. In these mice, the glomeruli exhibited an increase in mesangial matrix, more prominent in the vascular pole, but no tubular or interstitial abnormalities. While the association data seen in these high fat/high cholesterol-treated LCAT-deficient mice are suggestive of a link between LpX and the development of glomerulopathy, they did not separate the confounding contribution of the co-existing hyperlipidemia For example, recent *in vitro* data by Lynn et al[19] suggested that serum VLDL is also capable of inducing MCP-1 expression in the mesangial cells, a cellular response similar to that elicited by LpX.[17]

The novel mouse model we report here has virtually eliminated the confounding hyperlipidemic components and our findings provide the most compelling *in vivo* evidence that LpX, in the context of LCAT deficiency, is a major causative factor of the renal lesions. In addition to mesangial matrix expansion in the glomeruli, there was an impressive time-dependent increase in the number of foam cells within the glomerular tuft, and most of the foam cells were present at the vascular pole of the glomeruli. Increased RhoA immunostaining in the glomeruli was a novel finding of the current study. RhoA expression, like the mesangial matrix expansion and foam cells, was especially prominent in the vascular pole of the glomerulus.

Rho family proteins are GTPases and signaling molecules linked to actin cytoskeleton organization and cell proliferation.[20–22] More recently, Rho family proteins have also been linked to the pathogenesis of renal injury.[23] For example, inhibition of Rho kinase, one of the downstream effectors of RhoA, has been shown to reduce tubulointerstitial injury in the unilateral ureteral obstruction model of tubulointerstitial renal fibrosis.[23] Hemodynamic forces, like glomerular capillary pressure, are critical determinants of glomerulosclerosis, and sclerotic lesions often begin in the vascular pole of the glomerulus. *In vitro* studies have linked activation of RhoA to hemodynamic forces in mesangial cells.[24] We therefore performed immunohistochemistry to study RhoA staining given the prominent changes seen in the vascular poles of glomeruli in the S+lcat−/− mice. Although RhoA is biologically active when present in the active GTP-bound state, but not in the cytosolic GDP-bound state, our observation of a marked positivity in RhoA abundance by immunohistochemistry in the S+lcat−/− mouse kidneys and a complete absence of RhoA in the S+lcat+/+ control suggest the possibility that a fraction of the RhoA immuno-active protein might exist in the active form. Further studies will be necessary to definitively establish the link of RhoA activation to the development of glomerulosclerosis in our mice.

Recent studies suggest that the glomerular epithelial cell (podocyte) injury plays an important role in the development of progressive glomerulosclerosis,[25] and our finding of electron dense cytoplasmic inclusions in podocytes is intriguing. Although there are no *in vitro* studies of the effect of LpX on podocytes, LpX does have direct effects on cultured glomerular mesangial cells.[12] Dense inclusions in podocytes were associated with focal areas of foot process effacement, and this finding is similar to changes that have been described in kidney biopsies from patients with LCAT deficiency[10,11]

It has long been of great interest to understand the origin of LpX particles. To date, spontaneous production of LpX has been described in cholestatic liver disease, complete LCAT deficiency, and a murine model of ferrochelatase deficiency.[26] In the case of cholestatic liver disease, a recent study on the mdr2 knockout murine model revealed that the p-glycoprotein on the hepatocyte canaliculi is necessary for the generation of LpX in the milieu of biliary obstruction.[14] It has been hypothesized that the biliary vesicles destined to be secreted into the canaliculi are being, through a yet unknown mechanism, re-transcytosed to the sinusoidal surface to enter the circulation. This study had established a direct role of the liver in the generation of LpX in cholestatic liver diseases. The presence of circulation LpX is highly prevalent among subjects with complete LCAT deficiency but little is known about their origin. Data available to date are consistent with the hypothesis that an over-production of hepatically derived VLDL or intestinally derived chylomicrons, in the absence of LCAT, may result in an accumulation of the excess FC and PL, resulting in the formation of LpX. This is further supported by the previous reports of the presence of LCAT activities directly on the non-HDL particles. When LDL receptor knockout mice and apoE knockout mice, both characterized by severe hyperlipidemia caused by defective clearance of apoB-containing particles, develop plasma accumulation of LpX when made LCAT deficient,[15,27] but only to a relatively minor degree. By contrast, the S+lcat−/− mice showed marked increase in circulating LpX despite being hypolipidemic, further attesting to the importance of

lipoprotein production rate as a modulator of the biogenesis of LpX. Future studies will be required to further delineate the mechanism of the biogenesis in LpX in LCAT-deficient state.

In summary, we reported here the generation of a novel LCAT-deficient mouse model in that the lipoproteins are dominated by the FC- and PL-rich LpX vesicle. It appears that in the absence of LCAT, excess hepatic overproduction of lipoproteins may result in excess accumulation of the PL- and FC-rich vesicle. This mouse model has also provided the most compelling *in vivo* evidence that LpX plays an important role in the spontaneous development of a glomerulopathy, very similar to that seen in human LCAT deficiency. This lesion is characterized by glomerular foam cell infiltrates, glomerular lipid deposits, and progressive glomerulosclerosis.

Acknowledgments

We thank Eric Lam, Chunhui Xie, Maureen Lee, Baptista Calvieri, and Yun Lam for their excellent technical assistance.

References

1. Glomset JA: The plasma lecithins:cholesterol acyltransferase reaction. J Lipid Res 1968, 9:155–167
2. OK, Hill JS, Wang X, Pritchard PH: Recombinant lecithin:cholesterol acyltransferase containing a Thr123->Ile mutation esterifies cholesterol in low density lipoprotein but not in high density lipoprotein. J Lipid Res 1993, 34:81–88
3. Fielding CJ, Fielding PE: Molecular physiology of reverse cholesterol transport. J Lipid Res 1995, 36:211–228
4. Glomset JA, Mitchell CD, King WC, Applegate KA, Forte T, Norum KR, Gjone E: In vitro effects of lecithin:cholesterol acyltransferase on apolipoprotein distribution in familial lecithin:cholesterol acyltransferase deficiency. Ann NY Acad Sci 1980, 348:224–243
5. Ng DS, Francone OL, Forte TM, Zhang J, Haghpassand M, Rubin EM: Disruption of the murine lecithin:cholesterol acyltransferase gene causes impairment of adrenal lipid delivery and up-regulation of scavenger receptor class B type I. J Biol Chem 1997, 272:15777–15781
6. Steyrer E, Durovic S, Frank S, Giessauf W, Burger A, Dieplinger H, Zechner R, Kostner GM: The role of lecithin:cholesterol acyltransferase for lipoprotein (a) assembly: structural integrity of low density lipoproteins is a prerequisite for Lp(a) formation in human plasma. J Clin Invest 1994, 94:2330–2340
7. Narayanan S: Biochemistry and clinical relevance of lipoprotein X. Ann Clin Lab Sci 1984, 14:371–374
8. Glomset JA, Assmann G, Gjone E, Norum KR. The Metabolic and Molecular Bases of Inherited Disease. Edited by Scriver CR, Beaudet AL, Sly WS, Valle D. New York, McGraw-Hill, 1995, pp 1933–1951
9. Borysiewicz LK, Soutar AK, Evans DJ, Thompson GR, Rees AJ: Renal failure in familial lecithin:cholesterol acyltransferase deficiency. Q J Med 1982, 51:411–426
10. Imbasciati E. Paties C, Scarpioni L, Mihatsch MJ: Renal lesions in familial lecithin-cholesterol acyltransferase deficiency: ultrastructural heterogeneity of glomerular changes. Am J Nephrol 1986, 5:66–70
11. Lager DJ, Rosenberg BF, Shapiro H, Bernstein J: Lecithin-cholesterol acyltransferase deficiency: ultrastructural examination of sequential renal biopsies. Mod Pathol 1991, 4:331–335
12. Lynn EG, Siow YL, Frohlich J, Cheung GTOK: Lipoprotein-X stimulates monocyte chemoattractant protein-1 expression in mesangial cells via nuclear factor-kappa B. Kidney Int 2001, 60:520–532
13. Lambert G, Sakai N, Vaisman BL, Neufeld EB, Marteyn B, Chan CC, Paigen B, Lupia E, Thomas A, Striker LJ, Blanchette-Mackie J, Csako G, Brady JN, Costello R, Striker GE, Remaley AT, Brewer Jr HB, Santamarina-Fojo S: Analysis of glomerulosclerosis and atherosclerosis in lecithin cholesterol acyltransferase-deficient mice. J Biol Chem 2001, 276:15090–15098
14. Elferink RP, Ottenhoff R, van Marle J, Frijters CM, Smith AJ, Groen AK: Class III P-glycoproteins mediate the formation of lipoprotein X in the mouse. J Clin Invest 1998, 102:1749–1757
15. Ng DS, Maguire GF, Wylie J, Ravandi A, Xuan W, Ahmed Z, Eskandarian M, Kuksis A, Connelly PW: Oxidative stress is markedly elevated in lecithin:cholesterol acyltransferase-deficient mice and is paradoxically reversed in the apolipoprotein E knockout background in association with a reduction in atherosclerosis. J Biol Chem 2002, 277:11715–11720
16. Shimano H, Horton JD, Hammer RE, Shimomura I, Brown MS, Goldstein JL: Overproduction of cholesterol and fatty acids causes massive liver enlargement in transgenic mice expressing truncated SREBP-1a. J Clin Invest 1996, 98:1575–1584
17. Hammad SM, Hazen-Martin DJ, Sohn M, Eldridge L, Powell-Braxton L, Won W, Lyons TJ: Nephropathy in a hypercholesterolemic mouse model with streptozotocin-induced diabetes. Kidney Blood Press Res 2003, 26:351–361
18. Carlson EC, Audette JL, Veitenheimer NJ, Risan JA, Laturnus DI, Epstein PN: Ultrastructural morphometry of capillary basement membrane thickness in normal and transgenic diabetic mice. Anat Rec 2003, 271A:332–341
19. Lynn EG, Siow YLOK. Very low-density lipoprotein stimulates the expression of monocyte chemoattractant protein-1 in mesangial cells. Kidney Int 2000, 57:1472–1483
20. Bishop AL, Hall A: Rho GTPases and their effector proteins. Biochem J 2000, 348:241–255
21. Aznar S, Lacal JC: Rho signals to cell growth and apoptosis. Cancer Lett 2001, 165:1–10
22. Marimissen MJ, Chiariello M, Tanos T, Bernard O, Narumiya S, Gutkind JS: The small GTP-binding protein RhoA regulates c-jun by a ROCK-JNK signaling axis. Mol Cell 2004, 14:29–41
23. Nagatoya K, Moriyama T, Kawada N, Takeji M, Oseto S, Murozono T, Ando A, Imai E, Hori M: Y-27632 prevents tubulointerstitial fibrosis in mouse kidneys with unilateral ureteral obstruction. Kidney Int 2002, 61:1684–1695
24. Krepinsky JC, Ingram AJ, Tang D, Wu D, Liu L, Scholey JW: Nitric oxide inhibits stretch-induced MAPK activation in mesangial cells through RhoA inactivation. J Am Soc Nephrol 2003, 14:2790–2800
25. Kriz W, Lemley KV: The role of the podocyte in glomerulosclerosis. Curr Opin Hypertens Nephrol 1999, 8:489–497
26. Bloks VW, Plosch T, van Goor H, Roelofsen H, Baller J, Havinga R, Verkade HJ, van Tol A, Jansen PL, Kuipers F: Hyperlipidemia and atherosclerosis associated with liver disease in ferrochelatase-deficient mice. J Lipid Res 2001, 42:41–50
27. Ng DS, Xie C, Maguire GF, Zhu X, Ugwu F, Lam E, Connelly PW: Hypertriglyceridemia in lecithin-cholesterol acyltransferase-deficient mice is associated with hepatic overproduction of triglycerides, increased lipogenesis, and improved glucose tolerance. J Biol Chem 2004, 279:7636–7642